1   Experience-Driven Rate Modulation is Reinstated During Hippocampal Replay

2   Tirole M. [+][*], Huelin Gorriz M. [+][*], Takigawa M., Kukovska L., Bendor D.[*].

3   Institute of Behavioural Neuroscience (IBN), University College London (UCL), London, WC1H 0AP, UK

4   [+] These authors contributed equally

5   *Co-corresponding authors (margot.tirole.14@ucl.ac.uk, marta.huelin.16@ucl.ac.uk, d.bendor@ucl.ac.uk)

6

7   **Replay, the sequential reactivation of a neuronal ensemble, is thought to play a central**
8   **role in the hippocampus during the consolidation of a recent experience into a long-term**
9   **memory. Following a contextual change (e.g. entering a novel environment), hippocampal**
10   **place cells typically modulate their in-field firing rate and shift the position of their place**
11   **field, providing a rate and place representation for the behavioral episode, respectively.**
12   **However, replay has been largely defined by only the latter- based on the fidelity of**
13   **sequential activity across neighboring place fields. Here we show that dorsal CA1 place**
14   **cells in rats can modulate their firing rate between the replay of two different contexts,**
15   **mirroring the same pattern of rate modulation observed during behavior. This context-**
16   **driven rate modulation within replay events was experience-dependent, observable**
17   **during both behavioral episodes and throughout the subsequent rest period, but not prior**
18   **to experience. Furthermore, we demonstrate that both the temporal order and firing rate**
19   **of place cells can independently be used to decode contextual information within a replay**
20   **event, revealing the existence of two separable but complementary neural representations**
21   **available for memory consolidation processes.**

22

23   A key function of the hippocampus is the initial encoding and subsequent consolidation of
24   episodic memories. Hippocampal place cells are activated in sequential patterns during
25   behavioral episodes (e.g. a rodent running towards a goal), with each neuron's activity
26   modulated by the animal's position within an environment (i.e. a place field) (*1, 2*). During
27   offline periods such as sleep, place cells spontaneously reactivate, replaying the same
28   sequential pattern previously activated during the behavioral episode (*3–6*). This phenomenon
29   of neural replay is postulated to drive systems-level memory consolidation (*7–11*).
30   Hippocampal replay has largely been defined by the sequential patterns of place cells (*12, 13*),
31   which depends on the location of each neuron's place field in the environment (here referred
32   to as place representation). Yet, place cells also carry additional information in the magnitude
33   of their place field's activity (here referred to as rate representation). The magnitude of a place
34   field's activity (e.g. peak in-field firing rate) is modulated by both local and global contextual
35   cues (*14–17*), as well as behavioral variables (e.g. animal's acceleration during locomotion)
36   (*18, 19*), and cognitive events (e.g. animal's attention and perception) (*20–23*). However, we
37   do not know whether the hippocampus is capable of reinstating this rate modulation in place
38   cells during offline replay.

39 To address this question, we recorded extracellularly from the dorsal CA1 of rats (n= 3, male
40 Lister-hooded), trained to run back and forth along two novel linear tracks (2m) to collect a
41 liquid reward at each end (Fig. 1A, Fig. S1A, Table S1, see Methods). A view-obstructing
42 divider was placed between tracks and distinguishing visual cues were present within each
43 environment to facilitate contextual discrimination (and in turn, hippocampal remapping).
44 Additionally, rats rested in a quiet remote location, both before (PRE) and after (POST) the
45 exploration of the two tracks.
46
47 We observed global remapping of place cells between the two linear tracks [Pearson correlation
48 coefficient (r) between tracks population vectors, $r = 0.04 \pm 0.11$], such that the majority of
49 place fields shifted their location along the track and/or modulated their firing rate (i.e. changed
50 to higher or lower peak in-field firing rate) (Fig. S1B). Both the context (which linear track)
51 and current position (location of the animal on the linear track) could be inferred from place
52 cell activity with high accuracy using a naïve Bayes decoder (Fig. 1B, Fig.S1C). Track
53 detection accuracy exceeded 89% during RUN periods on both tracks [all sessions: 89 ± 5 %]
54 with an average median error of 5cm [all sessions: 5.17 ± 0.69 cm], while a population vector
55 analysis showed high correlation between the ratemaps of the first and second half of running
56 within each track [Pearson correlation coefficient (r) within track population vectors, $r= 0.83$
57 ± 0.04]. We also used Bayesian decoding to detect replay sequences of each linear track (Fig.
58 1B), with statistically significant replay trajectories identified by comparing the weighted
59 correlation score obtained from the posterior probabilities of each decoded event to three types
60 of event shuffles [Total replay events = 2805, PRE: Track1= 35±20, Track2= 37±15, POST:
61 Track1= 138±61, Track2= 156±34, RUN: Track1= 98±20, Track2= 95±31, Fig. S2, see
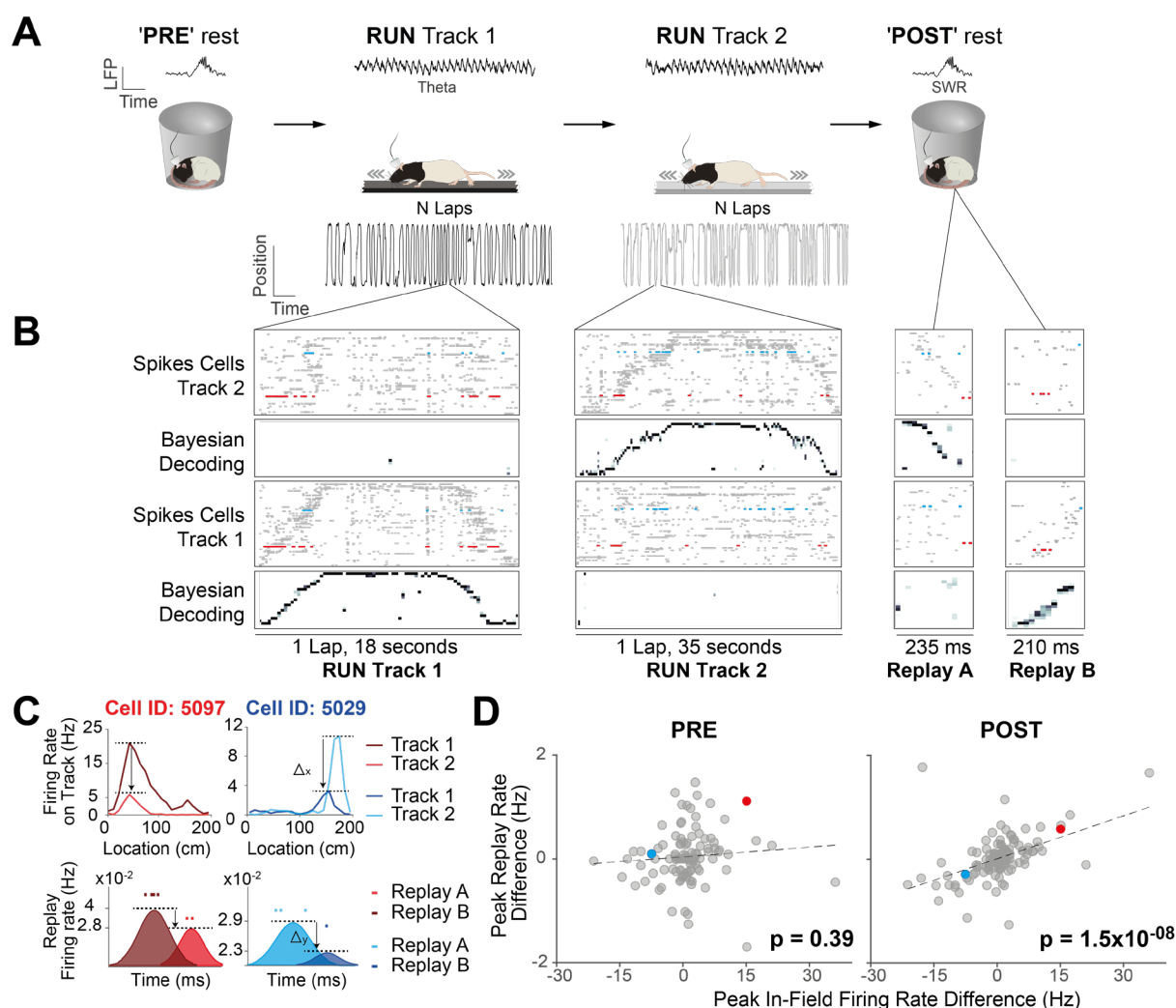62 Methods].

Figure 1. Rate coding in wake and rest. (**A**) Experimental design. Each recording session, the rats rested (PRE), ran back and forth on two different linear tracks (RUN), and then rested again (POST) (left to right). An example of LFP activity in each behavioral state is displayed [RUN-theta, PRE/POST-sharp wave ripples (SWR)] (**B**) Raster plots of spiking activity of cells sorted by their peak firing rate on the track (top: Track 2, bottom: Track 1), and the associated decoded positions for a single exemplar lap (first two columns) and replay event (last two columns), for each track (top: Track 2; bottom: Track 1). Example from Rat 3, session 2. (**C**) Two example neurons (highlighted in B) that changed their peak instantaneous firing rate (bottom) during two example replay events (displayed in B) in the same direction as their peak in-field firing rate difference (top). The activity and properties of the example neurons are color coded throughout all the panels. (**D**) The peak in-field firing rate difference (Track1-Track2) significantly predicts the average peak instantaneous replay rate difference (Track1-Track2) in POST rest, but not PRE rest. Each data point is a neuron active on both tracks (PRE: n = 106 cells, POST: n = 123 cells).

First, we sought to investigate whether the contextually-driven place fields' rate modulation between tracks is conserved during offline replay. Using all place cells active on both tracks and stable across the whole run (Fig.S1B, see Methods), we regressed the place fields' peak

3

82   in-field firing rate differences between tracks (Track1-Track2) against the difference (Track1-
83   Track2) in average peak instantaneous rate of those same cells during significant replay events
84   (Fig. 1C). For replay events during POST (but not PRE), the difference in peak in-field firing
85   rate between tracks was predictive of the difference in average peak instantaneous rates during
86   replay events from both tracks [PRE: β= .06, $F_{(1,104)}$=0.75, $P = 0.39$, R2= .007; POST: β=
87   .04, $F_{(1,121)}$= 36.95, $P < 0.001$, R2= .23; Fig. 1D]. In other words, if a place field had a higher
88   firing rate on Track 2 (compared to Track 1), it also tended to have a higher mean firing rate
89   across all Track 2 replay events (compared to Track 1 events) during POST, but not during
90   PRE. This suggests that any contextually-driven rate modulation between two behavioral
91   episodes is maintained during offline replay. This observation was consistent when using a
92   more selective criteria of place field activity (e.g. place fields with higher minimum peak firing
93   rate or place cells with a single field) (Fig. S3, S4) as well as for alternative metrics for both
94   replay firing rate (e.g. mean number of spikes per replay event and median replay rate) (Fig.
95   S4) and place fields firing rate (e.g. place field's area under the curve) (Fig. S4). Furthermore,
96   as expected, selecting only cells that were classified as significantly rate modulated led to an
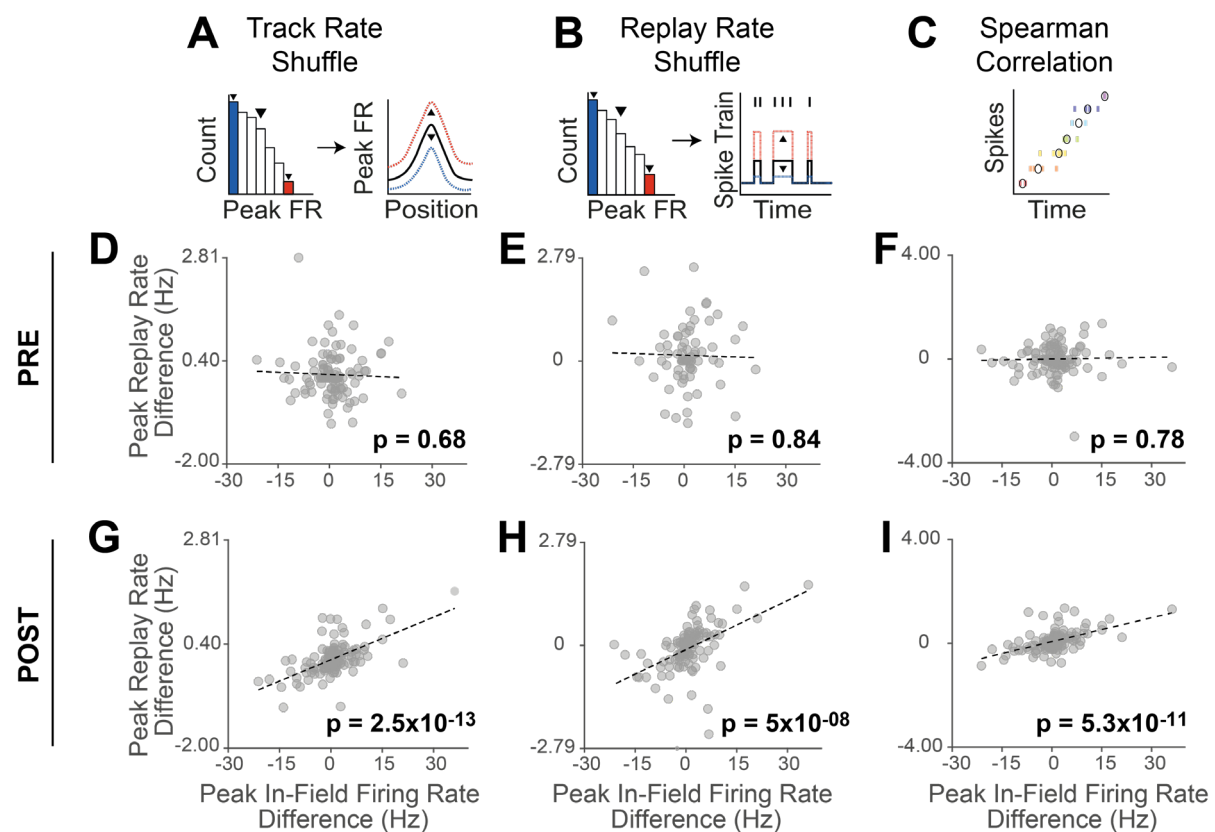97   even stronger effect (Fig. S4).
98

99

100   **Figure 2. The reinstatement of rate modulation during rest replay is observed using replay**
101   **detection methods insensitive to firing rate. (A-C)** Three methods of replay detection that are
102   insensitive to firing rate: **(A)** Track rate shuffle (PRE: n = 106 cells, POST: n = 123 cells), **(B)** Replay
103   rate shuffle (PRE: n = 69 cells, POST: n = 117 cells), **(C)** Spearman correlation (PRE: n = 111 cells,
104   POST: n = 123 cells). **(A-B)** Example of the original rate (in black) randomly scaled up (in red) or

105   down (in blue). **(D-F)** Regression of peak-in-field firing rate vs. peak replay rate difference (Track 1-
106   Track 2) for PRE replay events with modified detection method: **(D)** Track rate shuffle, **(E)** Replay rate
107   shuffle, **(F)** Spearman correlation. **(G-I)** Regression of peak-in-field firing rate vs. peak replay rate
108   difference (Track 1-Track 2) for POST replay events with modified detection method **(G)** Track rate
109   shuffle, **(H)** Replay rate shuffle, **(I)** Spearman correlation.

110

111   Replay detection methods generally detect the statistical significance of cells sequences based
112   on templates derived from the behavioral episode, which are sensitive to the order of place field
113   activation (during RUN and replay). However, because Bayesian decoding can also be
114   influenced by firing rate, we next tested whether firing rate differences between tracks may
115   bias the selection of the replay events used in the regression analysis. To remove the influence
116   of firing rate in the replay event selection, we employed two independent types of shuffles
117   before repeating the detection of replay events: 1) randomizing the overall firing rate of place
118   fields within a track (Track rate shuffle, Fig.2A) and 2) randomizing the cell's firing rate during
119   replay events (Replay rate shuffle) (Fig. 2B). For both shuffles, each place cell's firing rate was
120   scaled based on a value randomly drawn from the corresponding rate distribution obtained from
121   all cells. These significant replay events were then used to repeat the regression analysis using
122   their original content (i.e. the original replay spike train, instead of the shuffled one) against
123   the original differences in the place fields' in-peak firing rate. For both shuffles, we observed
124   a significant contextual rate modulation of replay, where track differences in the place fields'
125   in-peak firing rate remained predictive of track differences in the average peak instantaneous
126   rates during replay events in POST, but not PRE [PRE: Track rate shuffle $P = .68$, Replay rate
127   shuffle: $P = .84$, POST: Track rate shuffle $P < .001$, Replay rate shuffle: $P < .001$; Fig.
128   2D,E,G,H]. As an additional control, we detected replay events using a rank order correlation
129   method independent of Bayesian decoding, which relies only on comparing the median spike
130   times (across place cells) within a replay event compared to the sequential order of place field
131   activity along the track (Fig. 2C). Repeating the regression analysis based on the track
132   differences in the place fields' in-peak firing rate against the replay events detected using a
133   Spearman correlation still resulted in a significant contextual rate modulation of the replay
134   events rate in POST, but not PRE [PRE: $\beta = .002$, $F(1,111) = .08$, $P = .78$, $R2 = .0007$, POST:
135    $\beta = .03$, $F(1,121) = 51.99$, $P < .001$, $R2 = 0.3$; Fig. 2F,I]. Overall, these results indicate that the
136   contextual rate modulation observed during replay is not a result of a bias within the replay
137   detection analysis (namely, Bayesian decoding). Importantly, we did not observe any
138   significant track differences in place field or replay properties (Fig. S5, including the place
139   fields' peak in-field firing rate [two-sided two-sample KS test, $P = .62$] and replay average
140   peak instantaneous rate [two-sided two-sample KS test, $P = .79$], and confirmed that our
141   regression analysis was not influenced by any intrinsic biases between tracks by remeasuring
142   the statistical significance relative to a shuffled distribution (Fig. S6).

143

144   The phenomenon of replay has also been reported during awake quiescent states (e.g. while
145   pausing on the track), and it is thought to serve different functional roles, ranging from planning
146   to memory consolidation (*24–27*). We observed that during the behavioral episode on the

147   tracks, contextual rate modulation was expressed across local awake replay events [RUN: β=
148   .05, $F_{(1,120)}$= 197.02, $P < .001$, R2= .61; Fig. 3A]. The rate modulation during RUN was
149   stronger than the one observed in rest replay events during POST [β= .04, $F_{(1,121)}$= 36.95, P
150   < .001, R2= .23; Fig. 1D]. Place cells during RUN already showed evidence of contextual rate
151   modulation during awake local replay events within the first 2 laps of experience [2 laps: β=
152   .06, $F_{(1,8)}$= 5.91, P = .04, R2= .42; Fig. 3B]. Furthermore, place cells expressing rate
153   modulation during RUN replay events were also likely to show a similar direction of contextual
154   rate modulation (e.g. Track 1 > Track 2) during POST replay events [β= .78, $F_{(1,168)}$= 95.36,
155    $P < .001$, R2= .36, Fig. 3C], but not PRE [β= .02, $F_{(1,143)}$= 1.25, P = .2, R2= .008, Fig S7].
156   Contextual rate modulation during replay was significantly expressed throughout the entire rest
157   period during POST (at least 1 hour cumulatively, limited only by the maximum time period
158   tested), with the strongest effect observed in the earliest portion of POST rest (Fig. 3D).
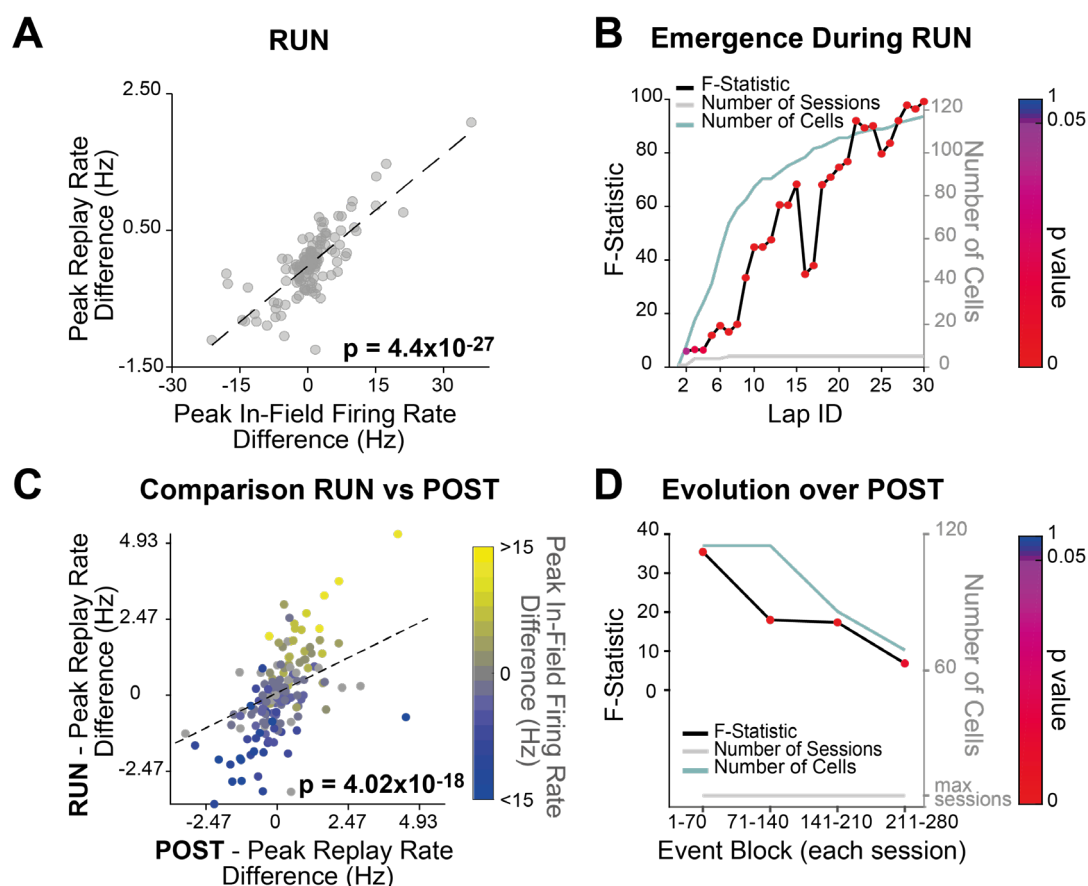159

160
161

162   **Figure 3. Rate modulation during replay is observed from the beginning of RUN and continues**
163   **throughout the entire RUN and POST epochs.** (**A**) Regression of peak in-field firing rates against
164   peak replay rates (track differences) for all local RUN replay events. (**B**) Lap by lap emergence of rate
165   modulation for RUN local replay events. F-statistic of regression - peak in-field firing rate vs. peak
166   replay rate (track difference) - for replay events occurring both prior to and including the specified lap
167   (lap ID). The p-value of each regression is indicated by color. The number of cells and number of data
168   sessions contributing in each regression are indicated with the green and grey line, respectively. (**C**)
169   Peak replay rate difference for replay events (RUN vs. POST), color coded by peak in-field rate

6

170 differences. (**D**) Temporal dynamics of rate modulation during POST. The regression's F statistic (y-
171 axis) and the corresponding p-value (marker color), analyzed in non-overlapping blocks of 70
172 consecutive replay events (per session).

173

174 Our data suggest that both place (i.e. sequences) and rate information is embedded within
175 hippocampal replay events. If this is the case, then the spatial context (i.e. track identity)
176 associated with a replay event should be identifiable using either the place or rate
177 representations alone. To address this question, we modified the current Bayesian framework
178 such that it would rely on either or both place and rate information. For each decoded replay
179 event, we measured the probabilistic bias towards one of the two tracks using the z-scored log
180 odd(*28*), ($\log \frac{\sum prob(Track_1)}{\sum prob(Track_2)}$). This method summed the decoded posterior probabilities for
181 each track within a replay event, quantified the log of the between track ratio, and then z-scored
182 this ratio relative to a shuffled distribution (Ratemap track label shuffle, see Methods). For
183 example, a more positive z-scored log odd would indicate a greater probabilistic bias towards
184 Track 1. Therefore, if the content of a replay event was detected for Track 1 (based on a
185 statistically significant sequence), the z-scored log odd for this event replay event would reflect
186 how well a place and/or rate representation could be used to correctly classify this replay event
187 as Track 1 (rather than Track 2).

188 In particular, we used two measurements to assess the replay track identity classification
189 performance when using either the rate and/or place representation: 1) the log odd difference
190 between two tracks compared to a Replay track identity shuffled distribution (see Methods)
191 and 2) the binary discriminability of a replay event's track identity using Receiver Operator
192 Characteristic (ROC) curves, in which the area under the ROC curve (AUC) of 0.5 indicates
193 chance discriminability (and an AUC of 1 indicates perfect discriminability). For both
194 measurements, only replay events with a statistically significant replay sequence were used.
195 When both place and rate information were unaltered, the z-scored log odd difference and the
196 track discriminability were significantly positive and highest for RUN [Δ(z-scored log odd)=
197 2.77, $P < .001$, AUC= .98], significant but marginally lower for POST [Δ(z-scored log odd)=
198 1.29, $P < .001$, AUC= .80], but indistinguishable from the null distribution and at chance levels
199 for PRE [Δ(z-scored log odd)= .08 , $P = .22$, AUC= 0.52] (Fig. 4A, Table S2).

200 We then proceeded to selectively remove either the place or firing rate information available
201 to the Bayesian decoder and assess its ability to determine the track being replayed. First, we
202 removed the firing rate information by setting each place field's in-field peak firing rate to its
203 average across both tracks, and by rescaling each cell's replay spike trains to its average firing
204 rate across all replay events (Fix rate manipulation). We found that place information alone
205 was sufficient to correctly classify replay events to each track, although both the z-scored log
206 odd difference and the AUC were slightly lower than when both place and firing rate
207 information were available [AUC difference < -0.1 compared to the original for all task periods,
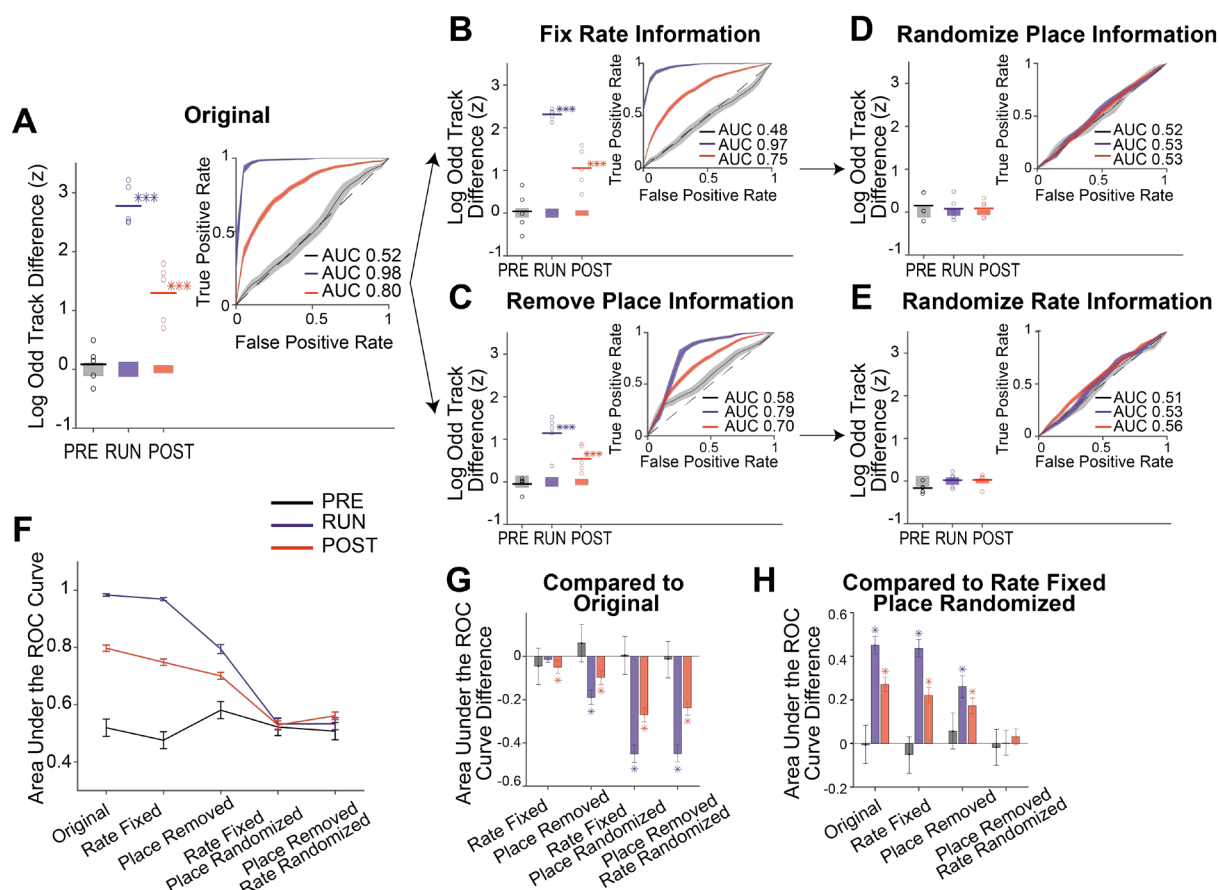208 Fig. 4B,F-H, Table S2].

7

Figure 4. Contextual information can be decoded from either place or rate representations during replay. (**A-E**) The decoding performance for context (Track 1 or Track 2) for each manipulation, restricting the information (rate and/or place) available to the decoder. (Main plots) Mean z-scored log odd difference between tracks for replay during PRE (black), RUN (blue) and POST (red). Each data point is the mean of an individual session, while the horizontal line indicates the mean across all sessions (*$P < 0.05$, **$P < 0.01$, ***$P < 0.001$, one-tailed). The filled box indicates the SEM from the Replay track identity shuffles. (Inset) ROC curves of Track1/Track2 binary discrimination for replay events during PRE, RUN and POST. The dashed line along the diagonal indicates chance performance (AUC = 0.5). The shaded region indicates the bootstrapped SE of the ROC curves. (**A**) Original (*rate and place information intact*) (**B**) Fix rate manipulation (*only place information available*) (**C**) Remove place manipulation (*only rate information available*) (**D**) Fix rate manipulation with place information additionally randomized (*no rate or place information available*). (**E**) Remove place manipulation with rate information additionally randomized (*no rate or place information available*). (**F**) Summary of mean AUC under each condition, for PRE, RUN, and POST (**G**) Mean AUC difference between original and each decoding manipulation. (**H**) Mean AUC difference between *negative control* and other conditions For G and H, * indicates where the 98.75% confidence interval of the bootstrapped AUC difference distribution does not overlap with 0 (see Table S3, S4). Similar results were obtained using an alternative approach (Delong method) for measuring significance (Table S5, S6, see Methods).

Next, we selectively removed place information without altering rate information, by expanding the size of our position and time bin for decoding: a single position bin spanning the

8

231 entire track and a single time bin spanning the entire replay event (Remove place manipulation,
232 Fig. 4C, F-H). This manipulation led to a significant log odd difference towards the correct
233 track and a high track discriminability for RUN [Δ(z-scored log odds)= 1.14, $P < .001$, AUC=
234 .79], POST [Δ(z-scored log odds)= .53, $P < .001$, AUC= .70], but not PRE (Δ(z-scored log
235 odds)= -.04, $P = 0.63$, AUC= .58], supporting the finding that rate modulation is reinstated
236 during replay and is experience-dependent. Finally, as a negative control for both
237 manipulations, where rate and place representations were disrupted, each remaining non-
238 manipulated representation (place or rate) was then randomized (Rate fixed place randomized
239 manipulation and Place removed rate randomized manipulation, respectively). Removing both
240 place and rate representations resulted in chance level discriminability for both conditions (Fig.
241 4D-H, Table S2).

242 Here we have shown that contextually driven place and rate representations used by the
243 hippocampus during behavior are reinstated during replay, with either representation being
244 sufficient to successfully decode the context being replayed. This phenomenon was experience-
245 dependent, as rate modulation within replay was only observed during and after a behavioral
246 episode, but not prior to it. While place cell sequences are generally stable across a behavioral
247 episode within a single environment, in-field firing rates can still increase (or decrease) with
248 minor contextual changes (*29*) a phenomenon referred to as rate remapping (*19*, *22*, *30*). Our
249 results suggest that during replay, firing rate modulation could allow the hippocampus to
250 discriminate between two marginally similar contexts even if they share an identical sequential
251 pattern of place cell activity.

252 Computational models of replay have commonly used modified synfire chains, sequentially
253 connected neurons that are often embedded within distinct recurrent networks (*31–33*). While
254 these models aim to replicate the sequential nature of replay, it remains to be seen whether they
255 can also reinstate experience-dependent rate modulation, or if additional mechanisms may need
256 to be considered. Compelling evidence suggests a key role for neocortical activity preceding a
257 hippocampal replay event, in determining its content (*10*, *34*, *35*). If cortical inputs to the
258 hippocampus during behavior underlie rate modulation (*36*), a reinstatement of these same
259 inputs prior to replay may be necessary for the subsequent rate modulation of hippocampal
260 place fields during offline states.

261

262

263 **AUTHOR CONTRIBUTIONS**

264 M.T.[1], M.H.G, and D.B. designed the experiment, M.T.[1] and M.H.G collected the data,
265 M.T.[1], M.H.G. and L.K. contributed to methodological development, M.T.[1], M.H.G, and
266 M.T.[2] analyzed the data, M.T.[1], M.H.G, M.T.[2], and D.B. wrote and revised the manuscript.

267 Order of co-first authorship was determined by coin-flip.

268 M Tirole[1], M Takigawa [2]

269

283   **REFERENCES**

284   1.   J. O'Keefe, J. Dostrovsky, The hippocampus as a spatial map. Preliminary evidence
285   from unit activity in the freely-moving rat. *Brain Res.* **34**, 171–175 (1971).

286   2.   J. O'Keefe, Place units in the hippocampus of the freely moving rat. *Exp. Neurol.* **51**,
287   78–109 (1976).

288   3.   A. K. Lee, M. A. Wilson, Memory of sequential experience in the hippocampus during
289   slow wave sleep. *Neuron* (2002).

290   4.   Z. Nádasdy, H. Hirase, A. Czurkó, J. Csicsvari, G. Buzsáki, Replay and time
291   compression of recurring spike sequences in the hippocampus. *J. Neurosci.* **19**, 9497–
292   9507 (1999).

293   5.   M. A. Wilson, B. L. McNaughton, Reactivation of hippocampal ensemble memories
294   during sleep. *Science (80-.).* (1994), doi:10.1126/science.8036517.

295   6.   W. E. Skaggs, B. L. McNaughton, K. M. Gothard, E. J. Markus, An Information-
296   Theoretic Approach to Deciphering the Hippocampal Code. *Proc. IEEE*, 1030--1037
297   (1993).

298   7.   G. Girardeau, K. Benchenane, S. I. Wiener, G. Buzsáki, M. B. Zugaro, Selective
299   suppression of hippocampal ripples impairs spatial memory. *Nat. Neurosci.* (2009),
300   doi:10.1038/nn.2384.

301   8.   I. Gridchyn, P. Schoenenberger, J. ONeill, J. Csicsvari, Assembly-Specific Disruption
302   of Hippocampal Replay Leads to Selective Memory Deficit. *Neuron*. **106**, 291–300
303   (2020).

304   9.   D. Ji, M. A. Wilson, Coordinated memory replay in the visual cortex and hippocampus
305   during sleep. *Nat. Neurosci.* **10**, 100–107 (2007).

306   10.   G. Rothschild, E. Eban, L. M. Frank, A cortical – hippocampal – cortical loop of
307   information processing during memory consolidation. *Nat. Neurosci.*, 1–12 (2016).

10

308   11.   A. Fernández-Ruiz, A. Oliva, E. Fermino De Oliveira, F. Rocha-Almeida, D. Tingley,
309   G. Buzsáki, Long-duration hippocampal sharp wave ripples improve memory. *Science*
310   *(80-.)*. **364**, 1082–1086 (2019).

311   12.   T. J. Davidson, F. Kloosterman, M. A. Wilson, Hippocampal Replay of Extended
312   Experience. *Neuron*. **63**, 497–507 (2009).

313   13.   L. Genzel, G. Dragoi, L. Frank, K. Ganguly, L. De La Prida, B. Pfeiffer, E. Robertson,
314   A consensus statement: defining terms for reactivation analysis. *Philos. Trans. R. Soc.*
315   *B Biol. Sci.* **375** (2020), doi:10.1098/rstb.2020.0001.

316   14.   M. L. Shapiro, H. Tanila, H. Eichenbaum, Cues that hippocampal place cells encode:
317   Dynamic and hierarchical representation of local and distal stimuli. *Hippocampus*. **7**,
318   624–642 (1997).

319   15.   J. O'Keefe, D. H. Conway, Hippocampal place units in the freely moving rat: Why
320   they fire where they fire. *Exp. Brain Res*. **31**, 573–590 (1978).

321   16.   P. Ravassard, A. Kees, B. Willers, D. Ho, D. Aharoni, J. Cushman, Z. M. Aghajan, M.
322   R. Mehta, Multisensory Control of Hippocampal Spatiotemporal Selectivity. *Science*
323   *(80-.)*. **340**, 1342–1346 (2013).

324   17.   X. Zhao, Y. Wang, N. Spruston, J. C. Magee, Membrane potential dynamics
325   underlying context-dependent sensory responses in the hippocampus. *Nat. Neurosci.*,
326   1–11 (2020).

327   18.   A. S. Etienne, K. J. Jeffery, Path integration in mammals. *Hippocampus*. **14**, 180–192
328   (2004).

329   19.   F. Savelli, J. J. Knierim, Origin and role of path integration in the cognitive
330   representations of the hippocampus: computational insights into open questions. *J.*
331   *Exp. Biol.* **222**, 1–13 (2019).

332   20.   A. A. Fenton, R. U. Muller, Place cell discharge is extremely variable during
333   individual passes of the rat through the firing field. *Proc. Natl. Acad. Sci.* **95**, 3182–
334   3187 (1998).

335   21.   L. M. Frank, E. N. Brown, M. Wilson, Trajectory Encoding in the Hippocampus and
336   Entorhinal Cortex. *Neuron*. **27**, 169–178 (2000).

337   22.   A. V. Olypher, P. Lánský, A. A. Fenton, Properties of the extra-positional signal in
338   hippocampal place cell discharge derived from the overdispersion in location-specific
339   firing. *Neuroscience*. **111**, 553–566 (2002).

340   23.   J. D. Monaco, G. Rao, E. D. Roth, J. J. Knierim, Attentive scanning behavior drives
341   one-trial potentiation of hippocampal place fields. *Nat. Neurosci.* **17**, 725–731 (2014).

342   24.   D. J. Foster, M. A. Wilson, Reverse replay of behavioural sequences in hippocampal
343   place cells during the awake state. *Nature* (2006), doi:10.1038/nature04587.

344   25.   K. Diba, G. Buzsáki, Forward and reverse hippocampal place-cell sequences during
345   ripples. *Nat. Neurosci*. **10**, 1241–1242 (2007).

346   26.   R. E. Ambrose, B. E. Pfeiffer, D. J. Foster, Reverse Replay of Hippocampal Place
347   Cells Is Uniquely Modulated by Changing Reward. *Neuron*. **91**, 1124–1136 (2016).

348   27.   H. Xu, P. Baracskay, J. O'Neill, J. Csicsvari, Assembly Responses of Hippocampal
349   CA1 Place Cells Predict Learned Behavior in Goal-Directed Spatial Tasks on the
350   Radial Eight-Arm Maze. *Neuron*. **101**, 119-132.e4 (2019).

351   28.   A. A. Carey, Y. Tanaka, M. A. A. van der Meer, Reward revaluation biases
352   hippocampal replay content away from the preferred outcome. *Nat. Neurosci.* **22**,
353   1450–1459 (2019).

354   29.   S. Leutgeb, J. K. Leutgeb, C. A. Barnes, E. I. Moser, B. L. McNaughton, M. B. Moser,
355   Neuroscience: Independent codes for spatial and episodic memory in hippocampal
356   neuronal ensembles. *Science (80-.)*. (2005), doi:10.1126/science.1114037.

357   30.   A. A. Fenton, R. U. Muller, Place cell discharge is extremely variable during
358   individual passes of the rat through the firing field. *Proc. Natl. Acad. Sci. U. S. A.* **95**,
359   3182–3187 (1998).

360   31.   M. Abeles, Role of the cortical neuron: integrator or coincidence detector? *Isr. J. Med.*
361   *Sci.* **18**, 83–92 (1982).

362   32.   M. Diesmann, M.-O. Gewaltig, A. Aertsen, Stable propagation of synchronous spiking
363   in cortical neural networks. *Nat. 1999 4026761*. **402**, 529–533 (1999).

364   33.   N. Chenkov, H. Sprekeler, R. Kempter, Memory replay in balanced recurrent
365   networks. *PLOS Comput. Biol.* **13**, e1005359 (2017).

366   34.   D. Bendor, M. A. Wilson, Biasing the content of hippocampal replay during sleep.
367   *Nat. Neurosci.* (2012), doi:10.1038/nn.3203.

368   35.   P. A. Lewis, D. Bendor, How Targeted Memory Reactivation Promotes the Selective
369   Strengthening of Memories in Sleep. *Curr. Biol.* **29** (2019), pp. R906–R912.

370   36.   C. Rennó-Costa, A. B. L. Tort, Place and grid cells in a loop: implications for memory
371   function and spatial coding. *J. Neurosci.* **37**, 3490–16 (2017).

372   37.   X. Sun, W. Xu, Fast implementation of DeLong's algorithm for comparing the areas
373   under correlated receiver operating characteristic curves. *IEEE Signal Process. Lett.*
374   **21**, 1389–1393 (2014).

375

376 **SUPPLEMENTARY FIGURES**

377

378
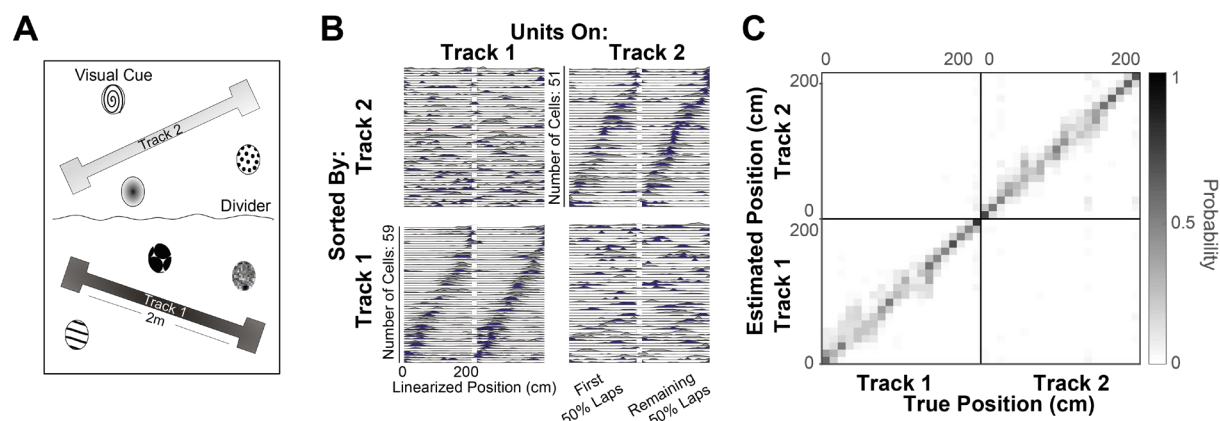
379 **Figure S1. experimental setup, remapping and field stability. (A)** Layout of the recording
380 room - two linear tracks, each surrounded by visual cues and visually occluded from each other. **(B)**
381 Ratemaps for Track 1 (left column) and Track 2 (right column) in an example session (rat 3, session 2)
382 computed for the first 50% of laps (left half) and last 50% of laps (right half) and sorted by the ordered
383 position of place fields on Track 1 (bottom) and Track 2 (top). **(C)** Confusion matrix for decoded
384 position (posterior probability normalized over both tracks) for an example session (rat 3, session 2).
385 Distribution of peak posterior probabilities (y-axis) is plotted at each True position during the behavioral
386 episode (x-axis).

387

388

13
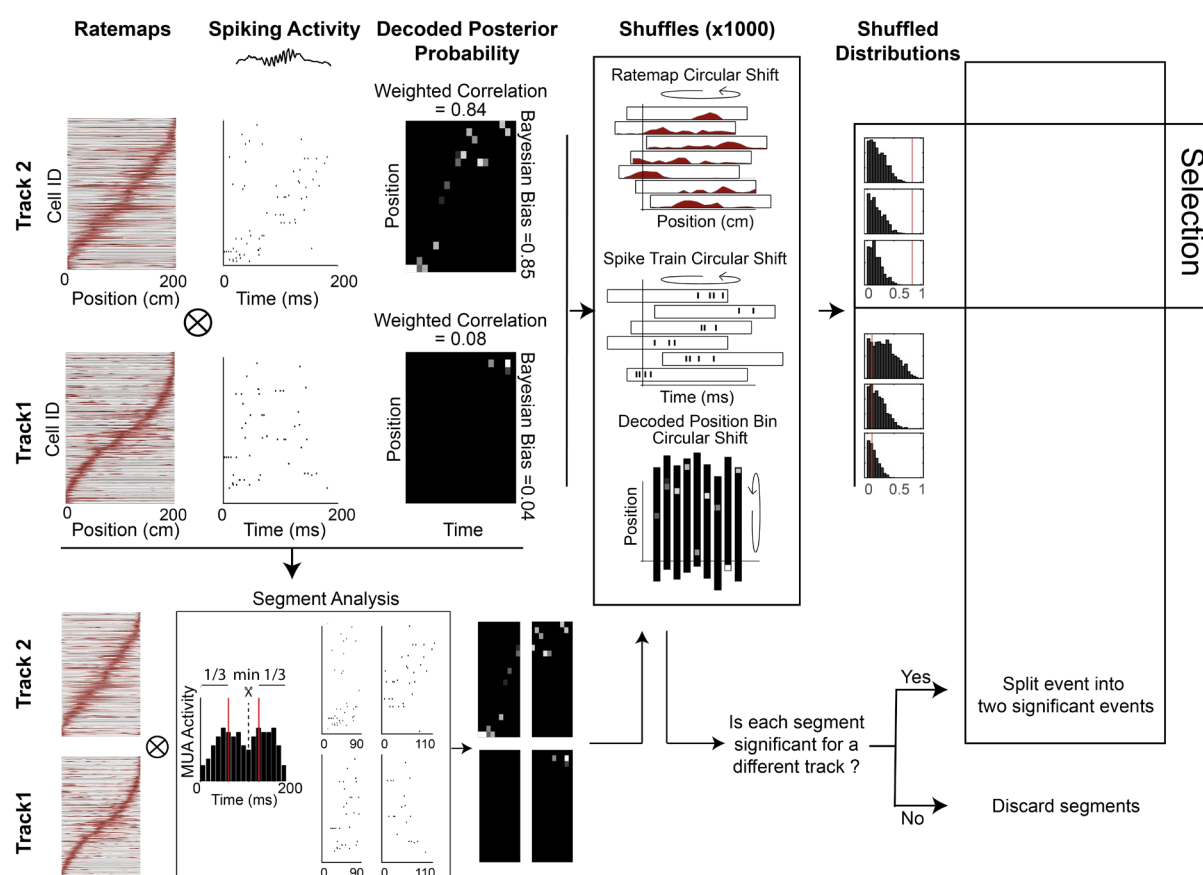
Figure S2. Analysis pipeline for detection of significant replay events. Detected replay spike trains were decoded using a Bayesian framework. Each track's ratemaps obtained during RUN were used to calculate the decoded posterior probabilities for each replay sequence (top left). In addition, all replay events were split into two shorter events based on the minimum in the MUA during the middle third of the replay event (bottom left, Segment analysis). For each replay event, weighted correlations were calculated on decoded posterior probability from both the whole replay sequence and each segment, and the three scores were compared to three different shuffles (ratemap circular shift, spike train circular shift, and decoded position bin circular shift, 1000 shuffles performed for each type). Only events with weighted correlation scores higher than 95% for every shuffle distribution (97.5% for split replay events) were considered statistically significant.
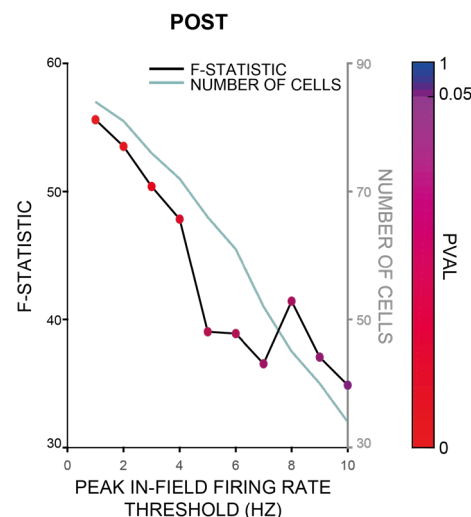
Figure S3. Significance of regression analysis using a stricter criterion of place cell activity. F-statistic of regression - peak in-field firing rate vs. peak replay rate (track difference) - for replay events occurring during POST rest, as the criterion for place cell activity (peak in-field firing rate) is progressively increased from 1 Hz. All regressions are statistically significant (up to and including using a threshold of 10 spk/s) The p-value of each regression is indicated by color. The number of cells used in each regression is indicated by the green line.

15
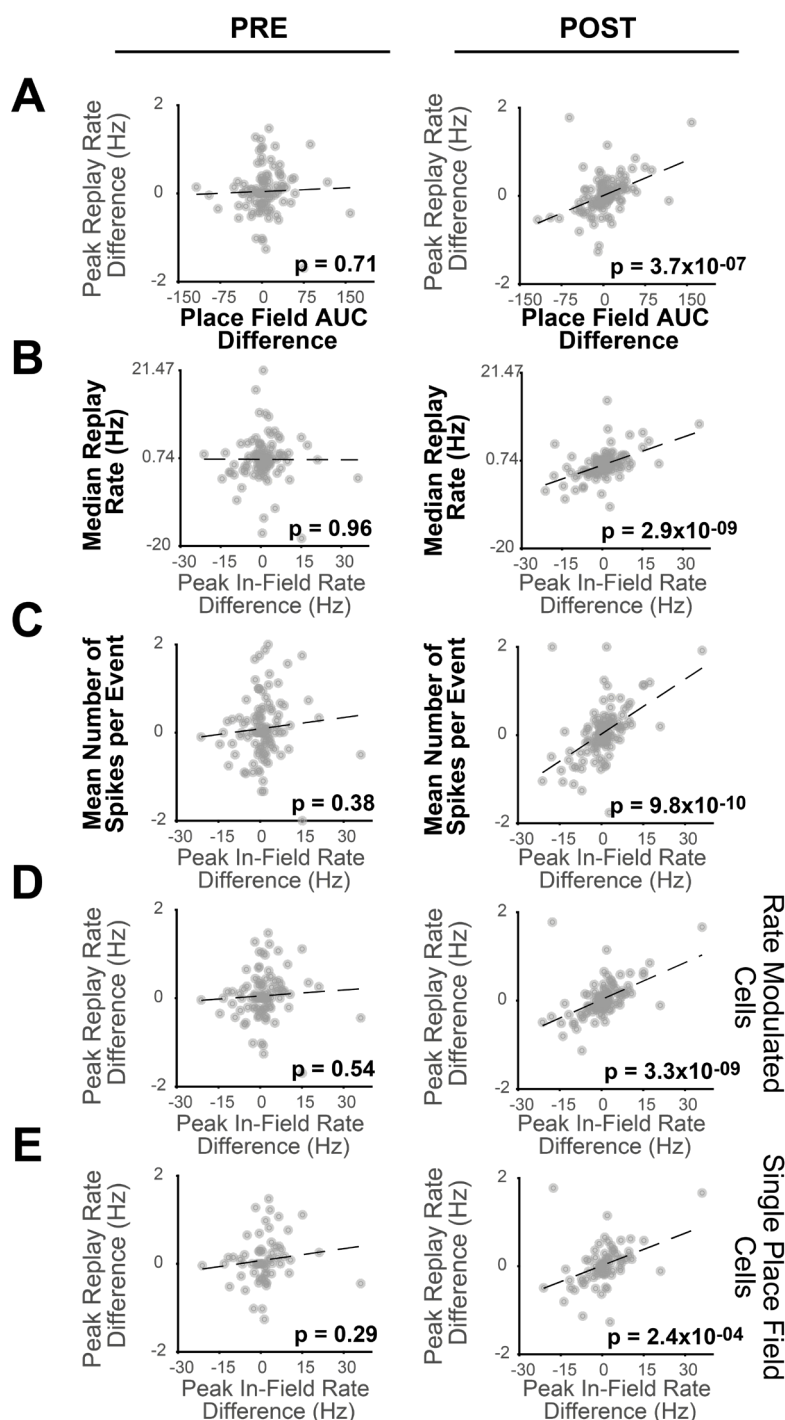
Figure S4. Significance of regression analysis with alternative place field and replay rate metrics, and stricter criteria for cell selection. F-statistic of regression - peak in-field firing rate vs. peak replay rate (track difference) - for replay events occurring during PRE (left column) and POST (right column) using alternative metrics and cell selection criteria. (**A**) Place field area under the curve (new x-axis, PRE: n = 106 cells, POST: n = 123 cells), (**B**) Median replay rate (new y-axis, PRE: n = 106 cells, POST: n = 123 cells), (**C**) Mean number of spike per event (new y-axis, PRE: n = 106 cells, POST: n = 123 cells), (**D**) Rate modulated cells (new criteria for cell selection, PRE: n = 97 cells, POST: n = 112 cells), (**E**) Single place field cells (new criteria for cell selection, PRE: n = 64 cells, POST: n = 77 cells).

16

Figure S5. Between track comparison of place field and replay properties. (A) Number of replay events (left) and replay event rate (right) for each track during PRE, RUN, and POST. The differences between tracks for any of these comparisons were not statistically significant (Wilcoxon sign rank, $P > 0.05$). **(B)** Distribution of Peak firing rate on track (top left), mean firing rate on track (top center), place field AUC (top right), median replay rate (bottom left), replay involvement (bottom center) and peak instantaneous replay rate (bottom right) for tracks 1 and 2, and for individual session distributions (inset) (K-S test, n.s $P > 0.05$).

Figure S6. Re-computing the statistical significance of regression analysis relative to a shuffled distribution. A Track rate shuffle (**A**) and Replay rate shuffle (**B**) were used to randomize the x-axis and y-axis respectively and create F-Statistic distributions for measuring significance of the regression. (**C-F**) Distribution of shuffle, dashed gray line: $P < 0.05$, red line: F-Statistic of original data (main plot). One example of a regression plot within the shuffle distribution (inset plot). (**C**) PRE: Track rate shuffle. (**D**) PRE: Replay rate shuffle. (**E**) POST: Track rate shuffle. (**F**) POST: Replay rate shuffle.
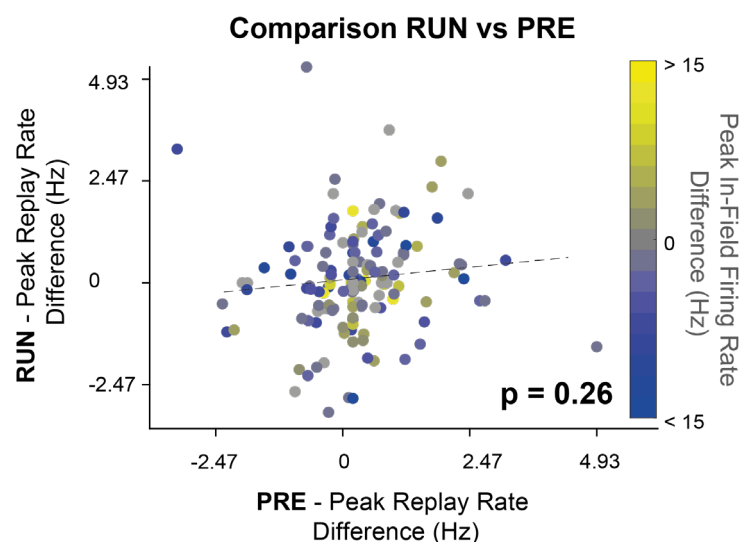
Figure S7. Between track differences in replay rate during PRE is not predictive of replay rate differences observed during RUN local replay events. Peak replay rate difference for replay events (RUN vs. PRE), color coded by peak in-field rate differences. A linear regression was not statistically significant ($P > 0.05$).

SUPPLEMENTARY TABLES

Table S1: Overview of behavior, number of recorded cells and decoding accuracy for all sessions and rats.

SESSION	TRACK	NUMBER OF LAPS	TIME RESTING (min)		CELLS			DECODING QUALITY (%)	
			PRE	POST	Total number of cells on track	Number of cells common to T1 and T2	Included cells in replay analysis	Classification accuracy	Local decoding accuracy
Rat 1	1	30	72	76	42	27	27	91	81
Rat 1	2	20	72	76	44	27	27	97	82
Rat 2, session 1	1	15	59	125	70	40	40	87	86
Rat 2, session 1	2	59	59	125	63	40	40	80	89
Rat 2, session 2	1	22	54	104	49	28	28	92	82
Rat 2, session 2	2	33	54	104	43	28	28	90	79
Rat 3, session 1	1	34	49	123	59	33	33	94	85
Rat 3, session 1	2	27	49	123	51	33	33	94	80
Rat 3, session 2	1	36	69	137	72	46	46	94	85
Rat 3, session 2	2	38	69	137	57	46	46	97	86

Table S2: Summary statistics of the z-scored log odd difference per session and across sessions for PRE, RUN and POST

463

	Session	Original			Rate fixed			Place removed			Rate fixed, Place randomized			Place removed, Rate randomized		
		Mean	SE	P value	Mean	SE	P value	Mean	SE	P value	Mean	SE	P value	Mean	SE	P value
PRE	1	-0.11		0.73	-0.02		0.56	-0.02		0.57	0.45		0.05	-0.30		0.92
	2	0.21		0.15	0.32		0.07	0.03		0.39	-0.21		0.80	-0.16		0.77
	3	-0.33		0.88	-0.54		0.96	-0.35		0.96	0.03		0.46	0.02		0.46
	4	0.15		0.32	-0.21		0.82	0.08		0.24	0.03		0.45	-0.15		0.73
	5	0.50		0.07	0.65		0.02	0.01		0.49	0.46		0.12	-0.25		0.73
	Mean	0.08	0.14	0.22	0.04	0.21	0.37	-0.05	0.08	0.64	0.15	0.13	0.11	-0.17	0.05	0.91
RUN	1	2.51		7.57×10^{-27}	2.13		9.24×10^{-26}	1.15		6.41×10^{-19}	0.01		0.48	-0.19		0.87
	2	3.22		9.61×10^{-36}	2.37		9.01×10^{-28}	1.39		2.05×10^{-28}	0.48		0.01	0.22		0.10
	3	2.55		5.93×10^{-23}	2.37		2.93×10^{-22}	1.27		5.08×10^{-18}	-0.19		0.78	0.12		0.22
	4	2.50		1.14×10^{-22}	2.44		1.38×10^{-22}	0.37		6.25×10^{-06}	-0.11		0.76	-0.15		0.79
	5	3.09		1.31×10^{-29}	2.26		4.38×10^{-25}	1.52		2.17×10^{-20}	0.20		0.16	0.09		0.29
	Mean	2.78	0.16	**1.08×10^{-121}**	2.31	0.06	**1.03×10^{-101}**	1.14	0.20	**9.23×10^{-29}**	0.08	0.12	0.18	0.02	0.08	0.43
POST	1	0.84		5.39×10^{-11}	0.43		1.09×10^{-05}	0.32		2.44×10^{-05}	0.17		0.09	0.15		0.18
	2	1.53		9.90×10^{-35}	1.03		1.96×10^{-24}	0.45		7.34×10^{-19}	0.33		0.003	0.10		0.15
	3	1.63		3.82×10^{-19}	1.44		3.30×10^{-16}	0.84		4.52×10^{-18}	-0.14		0.74	-0.25		0.98
	4	0.70		3.47×10^{-08}	0.78		5.46×10^{-11}	0.20		6.32×10^{-06}	0.20		0.03	0.09		0.20
	5	1.79		1.22×10^{-34}	1.59		9.58×10^{-30}	0.89		1.15×10^{-21}	-0.12		0.87	0.06		0.30
	Mean	1.30	0.22	**1.03×10^{-91}**	1.05	0.21	**1.98×10^{-74}**	0.54	0.14	**8.12×10^{-15}**	0.09	0.09	0.06	0.03	0.07	0.30

464 | | *Bold* values statistically significant

465

466   **Table S3: Summary statistics of the 98.75% confidence interval for the AUC difference between the original and the manipulated**
467   **condition**

		VS Original 98.75% confidence interval *BOLD values statistically significant from zero*		
		PRE	RUN	POST
Original VS rate fixed	**Mean AUC Diff**	-0.04	-0.02	-0.05
	SEM AUC Diff	0.04	0.01	0.02
	Lower CI	-0.15	-0.03	**-0.09**
	Upper CI	0.06	0.001	**-0.01**
Original VS Place removed	**Mean AUC Diff**	0.06	-0.19	-0.10
	SEM AUC Diff	0.04	0.02	0.02
	Lower CI	-0.04	**-0.23**	**-0.14**
	Upper CI	0.17	**-0.15**	**-0.06**
Original VS Rate fixed Place randomized	**Mean AUC Diff**	0.003	-0.45	-0.27
	SEM AUC Diff	0.04	0.02	0.02
	Lower CI	-0.10	**-0.51**	**-0.31**
	Upper CI	0.11	**-0.40**	**-0.23**
Original VS Place removed rate randomized	**Mean AUC Diff**	-0.01	-0.45	-0.24
	SEM AUC Diff	0.04	0.02	0.02
	Lower CI	-0.12	**-0.50**	**-0.28**
	Upper CI	0.09	**-0.40**	**-0.19**

468

469

470   **Table S4: Summary statistics of the 98.75% confidence interval for the AUC difference between the negative control (Rate fixed place**
471   **randomized manipulation) and the other conditions**

		VS Negative Control 98.75% confidence interval *BOLD values statistically significant from zero*		
		PRE	RUN	POST
Rate fixed VS Rate fixed Place randomized	**Mean AUC Diff**	-0.003	0.45	0.27
	SEM AUC Diff	0.04	0.02	0.02
	Lower CI	-0.11	**0.40**	**0.23**
	Upper CI	0.10	**0.51**	**0.31**
Place removed VS Rate fixed Place randomized	**Mean AUC Diff**	-0.05	0.44	0.22
	SEM AUC Diff	0.04	0.02	0.01
	Lower CI	-0.15	**0.38**	**0.17**
	Upper CI	0.06	**0.49**	**0.27**
Place removed VS Rate fixed Place randomized	**Mean AUC Diff**	0.06	0.26	0.17
	SEM AUC Diff	0.04	0.02	0.02
	Lower CI	-0.05	**0.20**	**0.12**
	Upper CI	0.17	**0.33**	**0.22**
Rate fixed, Place randomized VS Place removed rate randomized	**Mean AUC Diff**	-0.02	0.001	0.03
	SEM AUC Diff	0.04	0.03	0.02
	Lower CI	-0.11	-0.08	-0.02
	Upper CI	0.09	0.08	0.08

472

473

474 **Table S5: Summary statistics of the DeLong Test comparing the ROC curves between the original and the manipulated condition**

475

	DeLong Test versus Original (significance = 0.05/4 = 0.0125) (Bonferroni corrected) *BOLD values statistically significant*			
	Original VS Rate fixed	**Original VS Place removed**	**Original VS Rate fixed place randomized**	**Original VS Place removed rate randomized**
PRE	0.15	0.15	0.91	0.78
RUN	**0.007**	**5.56×10^{-34}**	**2.28×10^{-98}**	**6.92×10^{-100}**
POST	**8.15×10^{-08}**	**6.33×10^{-12}**	**2.65×10^{-55}**	**4.39×10^{-43}**

476

477

478   **Table S6: Summary statistics of the DeLong Test comparing the ROC curves between the original and the manipulated condition**

479

	DeLong Test versus Negative control (significance = 0.05/4 = 0.0125) (Bonferroni corrected) *BOLD values statistically significant*			
	Rate information fixed VS Rate fixed place randomized	**Place removed VS Rate fixed place randomized**	**Place information removed VS Rate fixed place randomized**	**Rate fixed, Place randomized VS Place removed rate randomized**
PRE	0.91	0.23	0.18	0.70
RUN	**2.28×10^{-98}**	**7.14×10^{-88}**	**1.17×10^{-23}**	0.96
POST	**2.65×10^{-55}**	**1.15×10^{-35}**	**2.03×10^{-20}**	0.09

480

METHODS

Animals

Three male Lister-Hooded rats (350-450g) were implanted with a microdrive with 24 independently moveable tetrodes. Prior to surgery, rats were kept at 90% of their free-feeding weight and housed in pairs on a 12-hour light/dark cycle, with 1 hour of simulated dusk/dawn. All experimental procedures and postoperative care were approved and carried out in accordance with the UK Home Office, subject to the restrictions and provisions contained within the Animal (Scientific Procedures) Act of 1986.

Surgery

Animals were deeply anaesthetized under isoflurane anesthesia (1.5-3% at 2L/min) and implanted with a custom-made microdrive array carrying 24 independently moveable tetrodes (modified from microdrive first published by (*12*)). Each tetrode consisted of a twisted bundle of four tungsten microwires (12μm diameter, Tungsten 99.95% CS, California Fine Wire), gold-plated to reduce impedance to < 200kΩ. One rat was implanted with a dual-hippocampal microdrive targeting both dorsal hippocampal CA1 areas (AP: -3.48mm, ML: +/-2.4mm from Bregma), each output carrying 12 tetrodes. The two remaining rats were implanted with a microdrive targeting the right dorsal hippocampal CA1 area (AP: 3.72mm, ML: 2.5mm from Bregma) and the left primary visual cortex (AP: -5.76mm, ML: -3.8mm from Bregma), using 16 and 8 tetrodes respectively. After surgery, animals were housed individually and allowed to recover with food and water *ad libitum* for a week before returning to being kept at 90% of their free-feeding weight.

Experimental design

A given recording session started with a 1-hour rest period in which the rats were placed in a quiet, remote location (rest pot), to which they had been previously habituated. The rest pot consisted of a black circular enclosure of 20cm of diameter, surrounded by a 50cm tall black plastic sheet that isolated them from the surroundings. Following the rest period, the rats were exposed to two novel 2m linear tracks in which they were allowed to run back and forth for 15 min, except for one session in which the animal ran for 30 min in the second track. Liquid reward was dispensed at each end of the track (0.1mL chocolate flavored soy milk) to encourage the animals to traverse the entirety of the track. In all except one session, the exposures to the two tracks were separated by a 10min rest period in the rest pot. The recording session finished with a final 2-hours rest period inside the rest pot.

To simulate novel environments, the shape of the tracks was changed between recording sessions and their surfaces covered with different textured fabrics. In each session, the room was surrounded by black curtains with different high contrast visual cues. The tracks were separated using view-obstructing dividers.

519

Spike detection and unit isolation

521 Spiking data was sorted using the semi-automatic clustering software KlustaKwik 2.0
522 (K.Harris, http://klustakwik.sourceforge.net/) and then manually curated with either Phy-GUI
523 (https://github.com/kwikteam/phy) or Klustaviewa (https://github.com/klusta-team/klustaviewa).
524 Putative single units were discriminated based on the spike waveform, a clean inter-spike interval,
525 and their stability across the recording session. The rest of the clustered activity was classified in
526 either multi-unit activity or noise.

527

LFP analysis

529 The power spectral density (PSD) of the LFP was calculated using Welch's method (*pwelch*,
530 MATLAB) to identify the channels with higher power for theta (4-12Hz) and ripple (125-
531 300Hz) oscillations, as well as the channel with the largest difference in normalized theta to
532 ripple power. The LFP of selected channels was next downsampled from 30 kHz to 1 kHz and
533 band-passed filtered (MATLAB command *filtfilt*). The instantaneous phases were estimated
534 using Hilbert transform.

535

Criteria for Place cell selection

537 Putative principal cells were identified by selecting units with a Half Width Half Max
538 (HWHM) larger than 500µs and mean firing rate <5Hz across the entire recording session. For
539 place cell classification, spike trains were speed-filtered to only include the spiking activity
540 between 4cm/s and 50cm/s. A principal cell was classified as a place cell according to the
541 following criteria: (1) the minimum peak firing rate was >1Hz in the unsmoothed ratemap and
542 (2) a stable spiking activity across the first half and second half of the exploration on the track.
543 Only place cells satisfying these two criteria for each linear track independently, were included
544 in the regression analysis (Fig. 1-3) and log odd analysis (Fig. 4).

545 To generate firing ratemaps (the spike histogram divided by the total dwell time at each position
546 bin), the position data was discretized in 2cm bins for visualization and plotting, and 10 cm
547 bins for Bayesian decoding. Only raw (unsmoothed) ratemaps were used for all Bayesian
548 decoding analyses.

549

Population vector analysis (PPV)

551 A population vector analysis was used to assess the ratemap stability for each track as well as
552 the degree of between track remapping (*29*). For each session, the linearized ratemaps of all
553 recorded pyramidal cells with a firing rate > 1Hz were stacked into a 20 position bins x N cells
554 matrix for each track. To assess remapping between tracks, the ratemaps computed from the
555 entire track experience were used, while to assess ratemap stability within a track, the middle

556   lap was used as a reference to compute separate ratemaps for the first and second half of the

557   behavioral episode. The population vector of rates at each position bin was then correlated with

558   its counterpart vector: either on the other track or during the other half of the experience. The

559   mean Pearson correlation value was first averaged across position bins and then across

560   sessions.

561

562   <u>Bayesian Decoding</u>

563   A naïve Bayesian decoding algorithm was applied to reconstruct the animal's spatial trajectory

564   during both behavior and replay events from CA1 hippocampal spiking activity (Zhang et al.,

565   1998):

566

$$P(x|n) = CP(x)\left(\prod_{i=1}^{N} f_i(x)^{n_i}\right) exp\left(-\tau \sum_{i=1}^{N} f_i(x)\right)$$

567   where P is the probability of the animal being at a specific position given the observed spiking

568   activity, C is a normalization constant, x is the subject's position, $f_i(x)$ is the firing rate of the

569   i^{th} place field at a given location x, and n is the number of spikes in the time window τ. The

570   normalization constant was re-defined as the summed posterior probabilities across both tracks.

571   The maximum probability of the subject's position was decoded using 250ms and 20ms time

572   bin during behavior and replay, respectively.

573   The decoding error was defined as the differences between the real location of the animal and

574   the estimated position with maximum-likelihood.

575

576   <u>Candidate replay event detection</u>

577   Candidate replay events were detected based on MUA and ripple power. MUA was first

578   smoothed with a Gaussian Kernel (sigma = 5 ms) and binned into 1 ms steps. Only MUA bursts

579   with a maximum duration of 300 ms and z-scored activity over 3 were selected. Ripples LFP

580   signal was smoothed with a 0.1 s moving average filter and a threshold over 3 was set for the

581   z-scored ripple power.

582   Candidate replay events passing both thresholds were next speed-filtered (above 5 cm/s), and

583   discarded if their sequence had less than 5 different units active or if their duration was below

584   100 ms or over 750 ms (thus, candidate events had at least 5 consecutive 20 ms bins). Events

585   detected within 50 ms were combined. In an effort to optimize detection of replay events and

586   avoid a minority of events that were discarded due to noisy probability decoding at the

587   beginning or the end of the event, candidate replay events were split in half. To do so, the

588   minimum MUA activity in the middle third of the candidate replay event was used determine

589   a natural midpoint to split the event in two segments. Both segments were decoded and tested

590   for significance independently following the same procedure as the 'intact' candidate replay

591 events (i.e., same criteria including minimum duration, etc.), for the exception of an adjusted
592 p-value threshold (P<0.025).

593 Replay events were classified as rest or awake local replay. Awake replay was defined as replay
594 events occurring while the animals were running on either of the tracks and classified as local
595 if the content of the replay event reflected the current track on which the animal was running.
596 Replay events detected during sleep or rest periods within the rest pot were classified as rest
597 replay events.

598

599 <u>Replay events scoring and significance</u>

600 Replay events were scored using weighted correlation between decoded posterior probabilities
601 across position and time.

602 Weighted mean:

603
$$m(x; prob) = \frac{\sum_{i=1}^{M} \sum_{j=1}^{N} prob_{ij} x_i}{\sum_{i=1}^{M} \sum_{j=1}^{N} prob_{ij}}$$

604 Weighted covariance:

605
$$cov(x, t; prob) = \frac{\sum_{i=1}^{M} \sum_{j=1}^{N} prob_{ij}(x_i - m(x; prob))(t_j - m(y; prob))}{\sum_{i=1}^{M} \sum_{j=1}^{N} prob_{ij}}$$

606 Weighted correlation:

607
$$corr(x, t; prob) = \frac{cov(x, t; prob)}{\sqrt{cov(x, x; prob)cov(t, t; prob)}}$$

608 Where x_i is the ith position bin, t_j is the jth time bin and $prob_{ij}$ is the probability at the position
609 bin i and time bin j.

610

611 The statistical significance of the weighted correlation for each candidate replay event was
612 assessed by comparison with three different 1000 shuffle distributions:

613 1) Spike train circular shift, in which the spike count vectors for each cell were independently
614 circularly shifted in time within each replay event, prior to decoding.

615 2) Place field shift, in which each ratemap was circularly shifted in space by a random amount
616 of position bins prior to decoding.

617 3) Circular shift of position, in which posterior probability vectors for each time bin were
618 independently circularly shifted by a random amount.

619 If the score of the candidate event was greater than the 95th percentile of the distribution for
620 all three shuffles then the event was considered to be significant.

621

Reinstatement of rate modulation analysis

623 Linear regression was used to measure the reinstatement of rate modulation between place
624 fields on the track and replay events (MATLAB function *fitlm*). For each place cell active in
625 both tracks, rate modulation on the track was measured by calculating (1) the difference in peak
626 in-field rate across tracks, and (2) the difference in the area under the curve (AUC; MATLAB
627 function *trapz*). Place fields with a peak in-field rate < 1 Hz on either track were excluded. As
628 a control, a variation of the analysis was done by excluding all cells with multiple place fields
629 on the same track. Multiple peaks for a single cell were considered to be different place fields
630 when their peak firing rate > 1 Hz, each place field width was over 2 spatial bins (20 cm) and
631 the distance between the peaks was of 4 spatial bins (40 cm).

632 Rate modulation during replay events was calculated as the change in each cell's firing activity
633 between the replay events encoding for each track. Included cells had to participate in at least
634 one replay event for each track. The firing rate change was measured as (1) the difference in
635 the average peak instantaneous rate across tracks, (2) the difference in the median rate across
636 replay events, and (3) the difference in the mean number of spikes across replay events.

637 To obtain the peak instantaneous rate of each event, each cell's spike train was binned into 1ms
638 steps, filtered with a 100ms long Gaussian window with σ=20ms (MATLAB command *filter*),
639 and the peak amplitude of the resulting signal measured.

640

Controls for replay detection analysis

642 Two types of shuffles were applied to the data before repeating the detection of replay events
643 using Bayesian decoding: a Track rate shuffle and Replay rate shuffle. The Track rate shuffle
644 consisted in the randomization of the firing rate of the place fields within a track, while the
645 Replay rate shuffle randomized the cells' firing rate during the replay events. For both shuffles,
646 each place cell's firing rate was scaled based on a value randomly drawn from a distribution of
647 firing rates obtained from the analyzed place cells on the track (for the Track rate shuffle) or
648 during the replay events (for the Replay rate shuffle). The shuffled data was then used to repeat
649 the detection of replay events, and the newly identified significant replay events were used in
650 a linear regression comparing their original spike content (instead of the shuffled one) against
651 the original differences in the peak in-field rate.

652

Remapping classification

654 A bootstrapping procedure was used to identify the rate and place modulation properties of
655 each cell. Modulation was defined when the track difference in a place field's specific
656 parameter (e.g. peak in-field firing rate or peak location) exceeded the intrinsic variability of
657 such parameter on a single track. The distribution of each parameter was computed for both
658 tracks by calculating firing ratemaps from a randomly sampled N out of N laps (1000 iterations,

659   with replacement). The median value of a track distribution was then compared to the $5^{th}/95^{th}$

660   percentiles of the other track, and vice versa. If either median exceeded either percentile, the

661   cell was classified as being modulated between tracks for that parameter.

662

663   <u>Sequenceless Bayesian Decoding</u>

664   The sequenceless Bayesian decoding was modified from Carey et al., (2019). Only cells with

665   stable place fields on the track in the first and second half of the behavioral episode (peak rate

666   > 1Hz) were included in our sequenceless decoding analysis.

667

668   Before Bayesian decoding, ratemaps for Track 1 and Track 2 were concatenated as a single

669   matrix [nCell x (nPosition(T1) + nPositions(T2))]. Unless otherwise mentioned, 20ms time

670   bins and 10cm position bins were used for decoding. After decoding, the posterior probabilities

671   for each time bin were normalized across all position bins on both tracks to sum to 1. Then, the

672   summed posterior probability across all time bins within each replay event was computed, and

673   the probabilistic bias towards Track 1 or Track 2 for each replay event was quantified as

674    $\log(\frac{\sum Prob(Track_1)}{\sum Prob(Track_2)})$ (log odds), where $\sum Prob(Track_1)$ and $\sum Prob(Track_2)$ referred to the

675   summed posterior probabilities for Track 1 and Track 2 respectively. To remove any intrinsic

676   probabilistic bias, each raw log odd calculation was then z-scored relative to a shuffled log odd

677   distribution (Ratemap track label shuffle), obtained by randomly permuting each cell's Track 1

678   and Track 2 ratemaps (either keeping a cell's ratemap unaltered or performing a between track

679   swap) 1000 times for each replay event.

680

681   To test decoding using place or rate representation alone, the original data were manipulated

682   as the following:

683   - Rate fixed manipulation: Rate information was fixed by rescaling each cell's peak in-field

684   firing rate to the mean value across both tracks, and its spike count in each replay event to the

685   average firing rate across all replay events.

686   - Place removed manipulation: The place (and sequence) information was removed by

687   decoding with only a single position bin, which encompassed the entire track (mean firing rate

688   on each track when speed is above 5cm/s) and a single time bin, which spanned the entire

689   replay event.

690

691   Two negative controls were included to disrupt both rate and place information:

692   - Rate fixed place randomized manipulation: After fixing rate information, place information

693   was randomized using cell ID shuffle in which all cells were randomly reassigned to a different

694   cell's ratemap for each replay event.

695   - Place removed rate randomized manipulation: After removing place information, rate

696   information was randomized by scaling the firing rate on each track based on a value

697   randomly drawn from a distribution of firing rates obtained from the analyzed place cells on

698   the track.

699

700

701   ROC analysis

702

703   The 'ground truth' track identity for each replay event was assigned based on the sequenceness
704   of the replay determined by weighted correlation and compare to three shuffled distributions.
705   The binary discriminability of a replay event's identity (Track1 or Track 2) during PRE, POST
706   or RUN was quantified using the Receiver Operative Characteristic (ROC) curve. By
707   systematically shifting the discrimination threshold along the z-scored log odd distributions for
708   Track 1 replay events and Track 2 replay events, a range of true positive rates and
709   corresponding false positive rates at each threshold was used to construct the ROC curve. A
710   trapezoidal approximation was used to estimate the area under each ROC curve (MATLAB
711   function *perfcurve* for both constructing ROC curve and estimating area under the curve). The
712   bootstrapped distributions of ROC curves and the area under the corresponding ROC curves
713   were produced by resampling with replacement 1000 times.

714

715   Statistics

716   Z-scored Log Odd significance

717   The statistical significance of the z-scored log odd difference between Track 1 and Track 2 was
718   determined by comparison with a shuffled distribution in which replay events were resampled
719   with replacement 1000 times and their track identities were randomly assigned. The single z-
720   scores were computed relative to the shuffled distributions, after which the associated one
721   tailed p-value was calculated. The log odd difference was considered significantly different
722   from the shuffled distribution at the significance level of 0.05.

723   Bootstrapping for ROC significance

724   To determine if rate and/or place representation manipulations significantly changed the area
725   under the curve (AUC) of the ROC curves, we calculated the confidence interval for the
726   difference between each condition's bootstrapped AUC distribution and that of the original
727   data. This was repeated later replacing the original data by one of the negative controls (rate
728   fixed or place randomized manipulation). The 98.75% confidence interval was used to account
729   for four comparisons (1-(alpha/n), where alpha=0.05 and n = 4) within the same behavioral
730   epochs. The mean difference between two bootstrapped AUC distributions were only
731   considered statistically significant when the confidence interval did not overlap with 0.

732   Delong Test for ROC

733   To determine if rate and/or place manipulations statistically significantly changed the AUC of
734   ROC curves within the same behavioral epochs, the AUC of each condition was compared with
735   the AUC of the original data or the negative control (rate fixed, place randomized). The
736   DeLong Test (*37*) was employed to perform pair-wise comparisons between two ROC curves,
737   a non-parametric test that accounted for the correlated nature of the data from the same epoch.
738   The DeLong variance-covariance matrix for two ROC curves was computed using MATLAB-

739   based algorithm [https://github.com/PamixSun/DeLongUI] developed by Sun and Xu (2014)

740   (36).

741   A z-score was calculated based on the following equation:

742

$$z = \frac{|AUC_A - AUC_B|}{\sqrt{var(A) + var(B) - 2cov(A,B)}}$$

743   The p value threshold for the statistical significance of the z-score was Bonferroni corrected to

744   account for multiple comparisons.

745

746   <u>Code Availability</u>

747   All analysis was carried out using MATLAB (Mathworks, Natick MA) and all code is available

748   from the authors upon reasonable request.